ACS OMEGA

http://pubs.acs.org/journal/acsodf

Article

A Switching-Type Positive Temperature Coefficient Behavior Exhibited by PPy/$(PhSe)_2$ Nanocomposite Prepared by Chemical Oxidative Polymerization

Tabee Jan, Masood Ahmad Rizvi,* Syed Kazim Moosvi, Mohd Hanief Najar,* Sajjad Husain Mir, and Ghulam Mustafa Peerzada

Cite This: *ACS Omega* 2021, 6, 7413−7421

Read Online

ACCESS | Metrics & More | Article Recommendations

ABSTRACT: In this study, we prepared a polypyrrole-diphenyl diselenide [PPy/$(PhSe)_2$] nanocomposite by oxidative chemical polymerization for the purpose of temperature sensing applications. Fourier transform infrared spectroscopy, X-ray diffraction and scanning transmission electron microscopy confirmed the synthesis of the above material. Thermogravimetry (TG) revealed enhanced thermal stability as compared to pristine polypyrrole (PPy). Dielectric study showed the material to have a dielectric constant of colossal value. The material has been found to exhibit correlated barrier hopping conduction (CBH) wherein hopping of charge carriers takes place over the insulating $(PhSe)_2$ barrier. The maximum barrier height was found to be 0.224 eV. The nanocomposite material was found to exhibit a switching-type positive temperature coefficient (PTC) behavior with a Curie temperature of 400 K. This has been explained by a CBH model wherein PPy chains expand upon heating, thereby reducing the barrier height to facilitate current flow. However, above 400 K, disruption of PPy chains allows to reflect a PTC behavior. This has been in agreement with TG data.

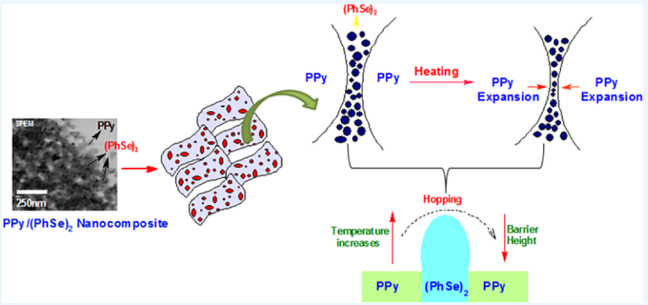

1. INTRODUCTION

Conductive polymer composite (CPC) materials have been explored for various applications such as antistatic materials,[1] electromagnetic interference shielding,[2−4] stretchable electronics and smart sensors,[5−7] etc.[8−12] However, recently, polymer-based composite materials were envisioned for thermistors that include both the characteristics of positive temperature coefficient (PTC) and negative temperature coefficient (NTC) effects of resistance.[13−16] A PTC effect refers to the increase in resistance with an increase in temperature, while an NTC is the decrease in resistance with the rise of temperature.[17,18] In addition to above two materials, switching-type PTC materials also exist in which an NTC effect occurs up to a certain temperature called Curie temperature, and then, an abrupt increase in resistance takes place with rise of temperature (PTC effect). The advantage of exploring conductive polymer composites (CPCs) for temperature sensing over those of traditional rigid ceramic thermistors lies in being lightweight with good processability, flexibility, and variety.[19−21] The materials of choice are usually semiconducting with a high degree of sensitivity that ranges from −3 to −6%/°C. Depending upon the materials choice and fabrication, they are generally used in the temperature range of −50 to 150 °C.

In most of the cases, electrically insulated polymer matrices are filled with conductive fillers such as carbon black (CB), carbon nanotubes (CNT), graphene, etc. for assessing their temperature sensing behavior. For instance, high-density polyethylene (HDPE) filled with multiwalled carbon nanotubes (MWCNTs) exhibits a PTC behavior,[22] and CNT-filled polydimethylsiloxane (PDMS) reflects an NTC property.[18] Similarly, chlorinated poly(propylene carbonate) (CPPC)/CB foams have been found to show a PTC behavior, while an NTC property has been exhibited for 2D graphene and polyamide 6 (PA-6)-filled ultrahigh-molecular-weight polyethylene (UHMWPE).[19,20] In addition, a Mn_3O_4-doped conductive polymer matrix, polyaniline, has been observed to show a low-temperature NTC behavior.[23]

Keeping this into consideration, we tried to use an insulating filler, viz., diphenyl diselenide (Ph_2Se_2), in a conductive polypyrrole (PPy) matrix for observing the temperature

Received: November 29, 2020
Accepted: February 8, 2021
Published: March 8, 2021

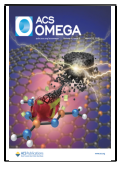

sensing behavior. Ph_2Se_2 is a high band gap system with a band gap of around 6.2 eV and - posses high chemical hardness.[24] Owing to its insulating nature, it can form potential barriers for electrical charge transport that is expected to be thermally activated. Moreover, the availability of vacant d orbitals in Se may help to interact with lone pairs present on N atoms of PPy chains. This would make the PPy chains more compact, which would further contribute to the thermal activation of charge carriers. It was found that the material exhibits a switching-type PTC behavior with a lower value of constant *B* in the NTC regime having a Curie temperature of around 400 K. This means that below the Curie temperature, the material allows current flow to cause a heating effect, while above that temperature, the increase in resistance hinders current flow to exhibit a cooling effect. This is essential for self-regulating heaters. For assessing the possible mechanism of charge transport in the present material such that the RT curve (resistance-temperature curve) follows explanation, a dielectric and impedance study has been carried out. From which, a correlated barrier hopping conduction (CBHC) has been observed.

2. RESULTS AND DISCUSSION

2.1. FTIR Characterization. FTIR spectra of PPy, $(PhSe)_2$, and the PPy/$(PhSe)_2$ nanocomposite are shown in Figure 1.The FTIR spectrum of PPy (Figure 1b) shows main characteristic peaks at 3404 cm^{-1} assigned to N−H stretching frequency, 1036 cm^{-1} is due to C−H in-plane bending vibration, 1489 cm^{-1} is assigned to C═C stretching, the peak at 1394 cm^{-1} is due to fundamental vibrations of the PPy ring, and 793 cm^{-1} is due to N−H in-plane deformation vibration. Some other peaks in the fingerprint region (600−1500 cm^{-1}) can be ascribed to the ring stretching and C−H in-plane deformation mode. The peaks obtained in the present study resemble that of previous work.[25] The FTIR spectra of $(PhSe)_2$ (Figure 1a) exhibit characteristic peaks at 1632 and 1564 cm^{-1} associated to phenyl groups, 1460 cm^{-1} owing to C═C aromatic vibration, 1023 cm^{-1} attributed to aromatic C−H stretching in-plane vibration, 994 and 732 cm^{-1} owing to aromatic C−H out-of-plane vibration, and at 680 cm^{-1}, which is attributed to aromatic C═C out-of-plane vibration mode.[26] The FTIR spectra of the PPy/$(PhSe)_2$ nanocomposite (Figure 1c) have peaks of both PPy and $(PhSe)_2$ with minor shifts indicating inclusion of $(PhSe)_2$ in the polymer matrix. The shifting of peaks in the nanocomposite may be explained by the initial adsorption of the pyrrole monomer over $(PhSe)_2$ particles. This is then followed by polymerization with constricted growth and restricted modes of vibration as compared to pristine PPy. As a result, the characteristic stretching frequencies are shifted.

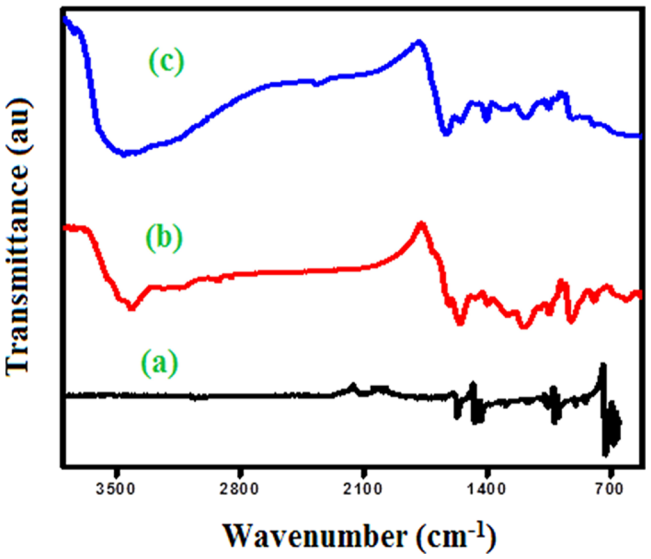

Figure 1. FTIR spectra of $(PhSe)_2$ (a), PPy (b), and PPy/$(PhSe)_2$ nanocomposite (c).

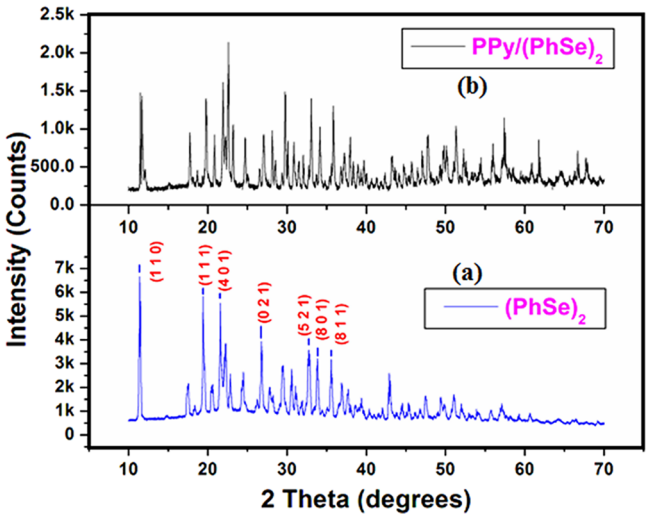

Figure 2. XRD patterns of $(PhSe)_2$ (a) and PPy/$(PhSe)_2$ nanocomposite (b).

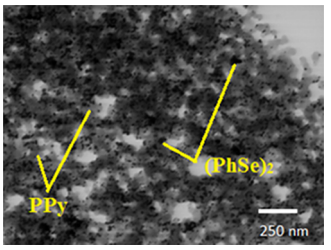

Figure 3. STEM image of the PPy/$(PhSe)_2$ nanocomposite.

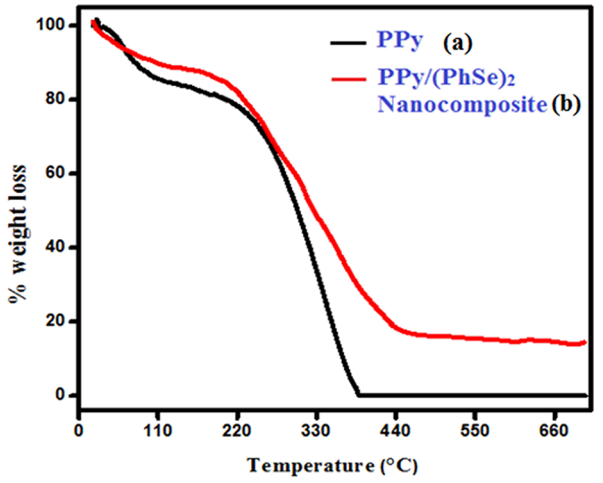

Figure 4. Thermograms of PPy (a) and PPy/$(PhSe)_2$ nanocomposite (b).

https://dx.doi.org/10.1021/acsomega.0c05799
ACS Omega 2021, 6, 7413−7421

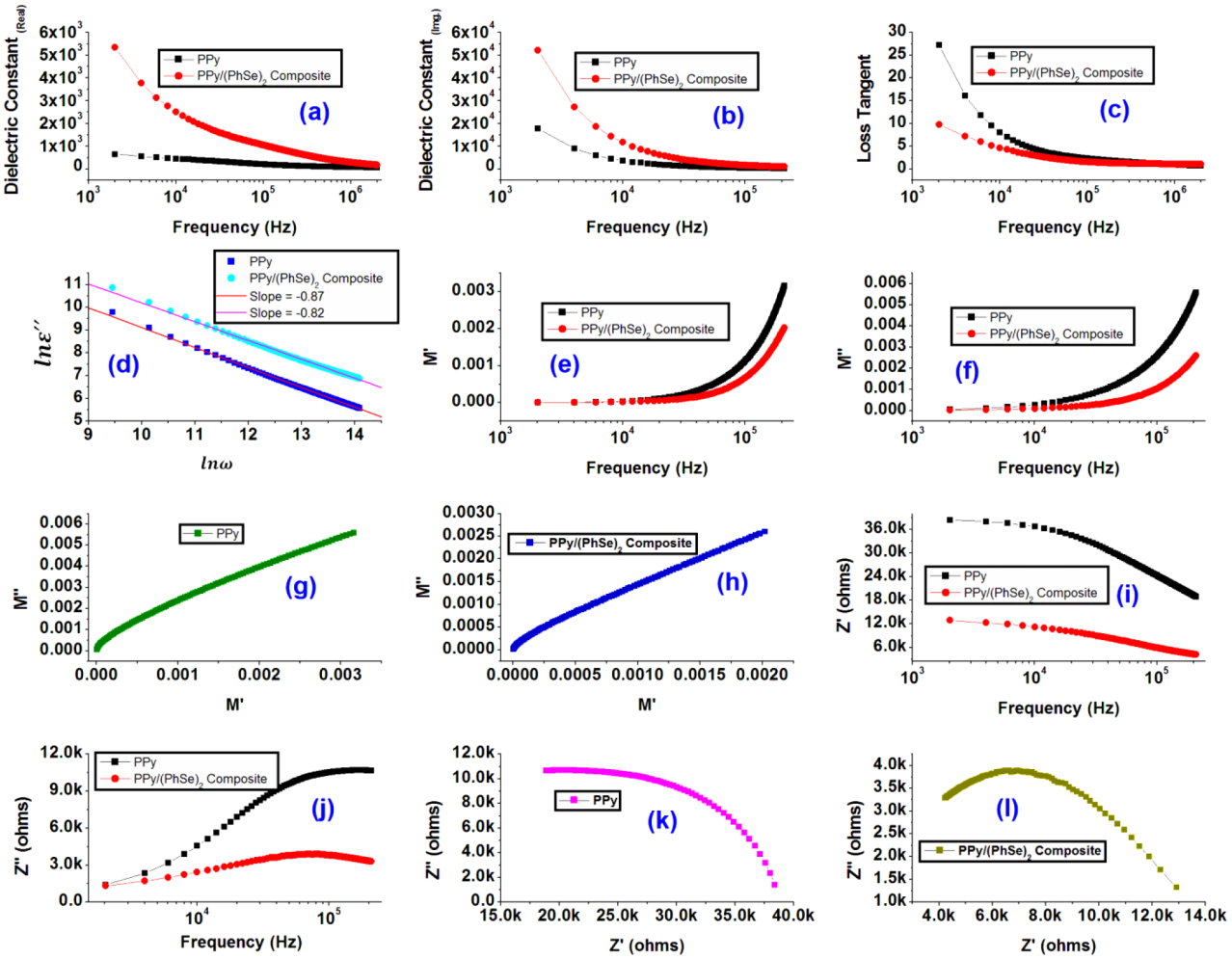

Figure 5. Variation of ε' (a, real), ε'' (b, imaginary), and tan δ (c, loss tangent) against frequency of the ac-field. Plot of ln ε'' against ln ω (d). Variation of M' (e), M'' (f), Z' (i), and Z'' (j) against the frequency of the ac-field. Cole−Cole plot in modulus formalism M'' vs M' (g,h) and in impedance formalism Z'' vs Z' (k,l).

2.2. X-ray Diffraction (XRD) Analysis. Figure 2 shows the X-ray diffraction pattern of the prepared $(PhSe)_2$ and PPy/$(PhSe)_2$ nanocomposite. Clearly, there are well-defined and sharp peaks with low FWHM indicating its crystalline nature. These sharp peaks were indexed using Powder-X software to analyze the crystal structure of $(PhSe)_2$. While indexing, $(PhSe)_2$ has been found to belong to an orthorhombic crystal system with a primitive (P) lattice (Figure 2a). The lattice parameters were found to be as follows: a = 23.9988, b = 8.2231, c = 5.6499, and $\alpha = \beta = \gamma = 90°$. These results were in accordance with values reported already in the literature.[27] The average crystallite size has been obtained to be 30.35 nm.

In the nanocomposite, the characteristic peaks of $(PhSe)_2$ overwhelm the amorphous nature of PPy (Figure 2b). This not only proved the successful synthesis of the PPy/$(PhSe)_2$ nanocomposite but can also make the material thermally more stable. This could be envisioned from thermogravimetry (section 2.4).

2.3. STEM Characterization. The morphology and shape of the PPy/$(PhSe)_2$ nanocomposite were characterized by STEM as shown in Figure 3. The STEM micrograph of the nanocomposite clearly showed that the networks of the nanocomposite, where synthesized polypyrrole is agglomerated in nanoparticle-like shapes connected with each other. The $(PhSe)_2$ (diphenyl diselenide) particles are granular spherical particles approximately 25−30 nm in diameter and are closely associated and coated on the network of the polypyrrole (PPy) matrix. The nanocomposite prepared by this strategy exhibited compact morphology and seemed more regular as evident from any agglomeration of the PPy matrix and the $(PhSe)_2$ particles. $(PhSe)_2$ is well-dispersed in the nanocomposite, and no free $(PhSe)_2$ nanoparticles are observed, which might be due to the string nucleating effect of PPy, resulting in a homogenous network of PPy around them.

2.4. Thermogravimetric (TG) Analysis. The TGA analysis of PPy and PPy/$(PhSe)_2$ is depicted in Figure 4. PPy shows two major weight loss steps (Figure 4a). The first step is observed between 70 and 110 °C, which indicates removal of water, residual organic solvents, and the pyrrole monomer. The second weight loss step starts from 200 °C that corresponds to degradation of PPy. The complete degradation of PPy occurs at 390 °C. The nanocomposite (Figure 4b) sample also shows two major weight loss steps. At 390 °C, about 29% of the nanocomposite is still left and thereby indicates its enhanced thermal stability in comparison to pure PPy. Since the organic constituents of polypyrrole are completely decomposed at 390 °C, the enhanced thermal stability of the nanocomposite may be attributed to the selenide content incorporated in the polymer matrix as the filler holds the PPy chains together in an ordered manner.[28]

https://dx.doi.org/10.1021/acsomega.0c05799
ACS Omega 2021, 6, 7413−7421

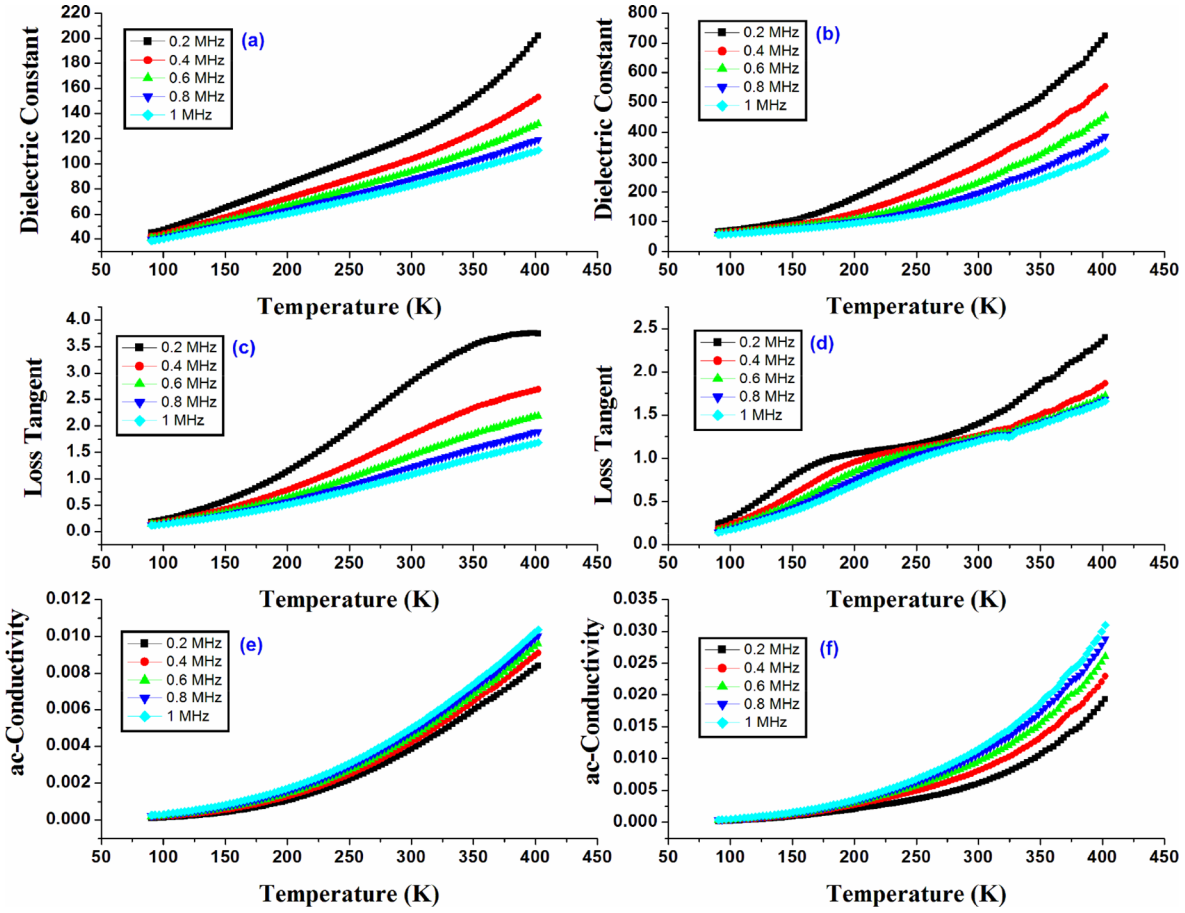

Figure 6. Variation of ε', tan δ, and ac-conductivity of PPy (a, c, and e) and PPy/$(PhSe)_2$ nanocomposite (b, d, and f) against temperature at various frequencies (0.2, 0.4, 0.6, and 0.8 MHz).

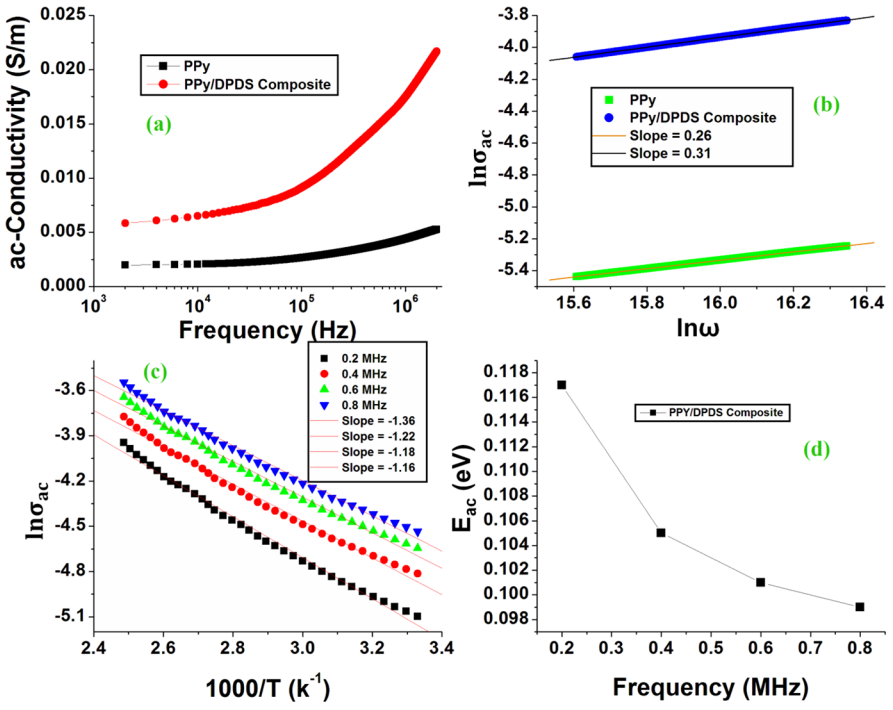

Figure 7. Variation of ac-conductivity against frequency (a), plot of ln σ_{ac} against ln ω (b), and ln σ_{ac} against inverse of temperature (c). Variation of activation energy (E_{ac}) against frequency of the ac-field (d).

https://dx.doi.org/10.1021/acsomega.0c05799
ACS Omega 2021, 6, 7413−7421

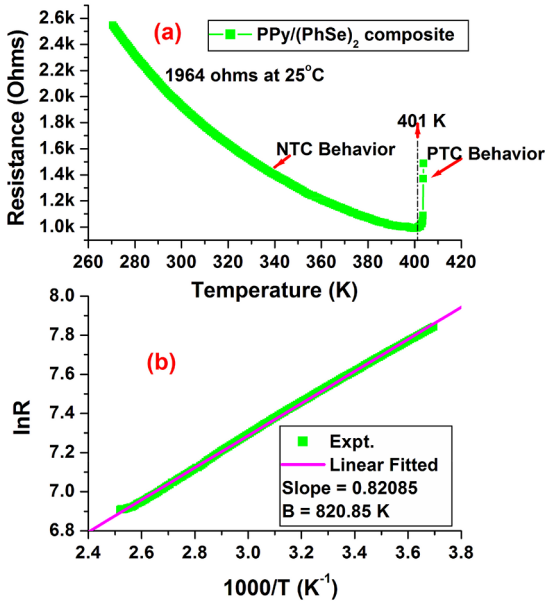

Figure 8. Variation of resistance with temperature of PPy/$(PhSe)_2$ nanocomposite (a) and plot of ln *R* against inverse of temperature for *B* determination (b).

Table 1. Various Parameters Corresponding to the NTC Regime for the PPy/$(PhSe)_2$ Nanocomposite

system	$B_{300-400K}$(K)	$I_{NTC(300-400K)}$	$\alpha_{T(300K)}$(%/K)	SC (/K)
PPy/$(PhSe)_2$ composite	820.85	2.554	−0.91	0.02

Scheme 1. Scheme Representing the Expansion of PPy in a Nanocomposite upon Heating (a) and Hopping of Charge Carriers over a Potential Barrier (b)

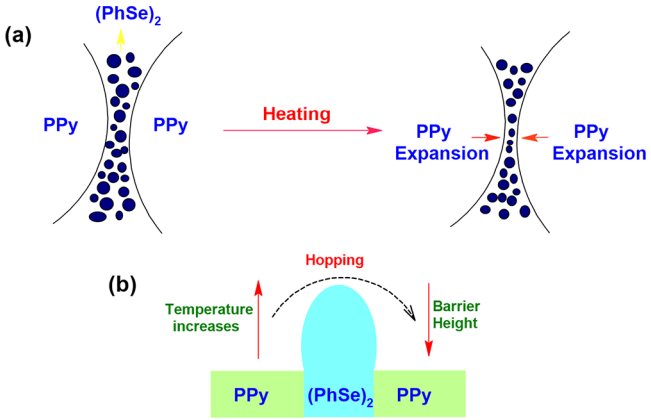

2.5. Dielectric and Impedance Spectroscopy. Figure 5 shows the variation of dielectric properties of the present material against the frequency of the ac-field. The dielectric constant (ε', real part) and dielectric losses (ε'' imaginary part and tan δ) show a normal dispersion behavior with increasing frequency of the applied field at room temperature. A high dielectric constant of colossal value ($>10^3$) in the given frequency range of 1 kHz to 0.1 MHz for the PPy/$(PhSe)_2$ nanocomposite can be attributed to the Maxwell−Wagner (MW) interfacial polarization in addition to other polarizations like electronic and dipolar orientation, etc. This is due to the heterogeneous nature of the material as is clear from STEM micrographs.[29] In comparison, pristine PPy chains exhibit a lower value of the dielectric constant in the given frequency range. This is because of the presence of $(PhSe)_2$, being a high band gap insulating system, in the PPy matrix (Figure 4a). This makes the nanocomposite material heterogeneous with a difference in resistivity. This difference in resistivity allows the constriction of charge carriers at phase boundaries to contribute to the interfacial polarization. With an increase in the ac-field, the dielectric constant decreases and finally attains a constant value. This is due to the relaxation phenomenon occurring in the nanocomposite material since at high frequencies, dipoles no longer follow the applied field.[30,31] Temperature variation of the dielectric constant (ε') for PPy and the PPy/$(PhSe)_2$ nanocomposite at various frequencies is shown in Figure 6a,b. Clearly in both cases, ε' is lower at low temperatures, and it increases as temperature rises. This is because the material is almost frozen at low temperatures, but as the temperature is increased, material movement commences to allow polarization and hence lead to an increased dielectric constant.[32] Moreover, temperature variation at low frequencies shows high ε' than at high frequencies. This is a usual behavior as dielectric relaxation takes place at high frequencies.

The dielectric loss (ε'' and tan δ) is contributed by (1) dipolar reorientation, which is characterized by a Debye-type dipolar loss peak, (2) dc-conduction losses characterized by $\varepsilon''_{dc} = \sigma_{dc}/\varepsilon_o\omega$, i.e., varying with angular frequency as ω^{-1} and without having any characteristic peak in the loss curve, (3) the loss due to interfacial polarization (Maxwell−Wagner (MW)-type or electrode polarization), and (4) vibrational losses, which occur at high frequencies.[33,34] The dielectric loss shows a decreasing trend with the frequency of the ac-field as shown in Figure 5b,c. Clearly, the absence of a Debye-type dipolar loss peak in the plot of tan δ against the ac-field indicated that the losses in the nanocomposite material may be dominated by the dc-conduction and interfacial losses. The dc-conduction losses in the nanocomposite material have been confirmed by the plot of lnε'' against lnω that revealed a straight line with a slope of around −0.82 (−0.87 for PPy), which is close to −1 as shown in Figure 5d. It is expected due to the absence of a loss peak in ε'' spectra that in turn suggests the masking of relaxations by the electrical conduction processes. This is also justified by the increase in dc-conduction (a high value of ε'' and constancy of σ_{ac} at low frequencies) while loading $(PhSe)_2$ in PPy, which may make PPy chains more compact to allow facile flow of charge carriers. This is well-supported by XRD. However, the slight variation in the slope of the lnε'' against lnω plot is indicative of the MW effect owing to the heterogeneous nature of the nanocomposite material wherein components differ in resistivity. The dielectric loss (tan δ) for the nanocomposite is lower than that of PPy that is in agreement with the higher dielectric constant in the PPy/$(PhSe)_2$ nanocomposite, which is an essential condition for it to be used in many technological applications. Figure 6c,d shows the temperature variation of tan δ at various frequencies. For both PPy and the PPy/$(PhSe)_2$ nanocomposite, tan δ increases with increase in temperature. This is because of increased movement of charge carriers and polarization as the temperature is raised that lead to the conduction and dipolar losses. At low temperatures, the motion is hindered, and dipoles are frozen to reflect low losses. Moreover, the losses are

https://dx.doi.org/10.1021/acsomega.0c05799
ACS Omega 2021, 6, 7413−7421

more at low frequencies than at high frequencies, which are due to the dielectric relaxations as already discussed.[35,36]

From electric modulus formalism as shown in Figure 5e,f, evidently, the approaching of M' to zero at low frequencies is indicative of the negligible contribution from electrode/interfacial polarization, and its increase with an increase in frequency suggests the occurrence of a dielectric relaxation phenomenon. Compared to PPy, the PPy/$(PhSe)_2$ nanocomposite undergoes relaxation at higher frequencies and thereby justifies its high dielectric constant. From the M'' vs frequency plot, it is expected to show a peaking nature at higher frequencies (as it goes out of scale). Frequencies to the left of the expected relaxation peak dictate long-range mobility of charge carriers corresponding to dc-conduction, while frequencies to the right of the expected relaxation peak indicate short-range mobility of charge carriers due to their confinement in potential wells corresponding to the ac-conduction. The expected relaxation peak represents a transition from dc- to ac-conduction.[37] In comparison to PPy, the nanocomposite exhibits the expected relaxation peak at a higher frequency with short height. This is indicative of higher capacitance over that of pristine PPy as peak height is inversely related to capacitance.[38] This has been attributed to the space charge interfacial polarization owing to heterogeneity of the nanocomposite material and thus supports the permittivity data.

The Cole−Cole plot in modulus formalism exhibits one semicircular arc for both PPy and PPy/$(PhSe)_2$ nanocomposites indicating a single relaxation [Figure 5g,h]. From impedance spectroscopy as shown in Figure 5i,j, Z' decreases with an increase in frequency for both PPy and the nanocomposite indicating the semiconducting nature of materials. Z'' on the other hand shows a peaking nature wherein the relaxation time (τ, corresponding to the frequency of the peak maximum f_{max}) has been calculated using the following equation

$$\tau = \frac{1}{2\pi f_{max}}$$

τ has been found to be longer for the nanocomposite than that of PPy. Shorter height of the relaxation peak for the PPy/$(PhSe)_2$ nanocomposite suggests a smaller value of resistance than PPy since peak height is directly related to resistance of the material.[39] This is justified from Cole−Cole plots also that reveal smaller semicircular arcs compared to PPy [Figure 5k,l].

2.6. Ac-Conductivity and Possible Conduction Mechanism. The variation of ac-conductivity with frequency for pristine PPy and the PPy/$(PhSe)_2$ nanocomposite is shown in Figure 7a. It is evident that conductivity runs parallel to the frequency axis (frequency independent region) at low frequencies indicating the dominance of dc-conduction involving long-range mobility of charge carriers. However, above a certain characteristic onset frequency called the hopping or critical frequency (ω_H), conductivity increases exponentially with the increase in frequency. This results into the short-range mobility of charge carriers corresponding to ac-conduction.[32,40] The dc-conductivity (σ_{dc}) of PPy and the PPy/$(PhSe)_2$ nanocomposite can be calculated by extrapolating σ values to low frequencies. It is observed that σ_{dc} is higher for the PPy/$(PhSe)_2$ nanocomposite (0.0057 S/m) than that of pristine PPy (0.0021 S/m). This may be attributed to the ordering of PPy chains upon nanocomposite formation for facile flow of current along with the increased number of charge carriers.

The overall conductivity (σ_t) of the nanocomposite material is given by the following relation

$$\sigma_t = \sigma_{dc} + \sigma_{ac}$$

or

$$\sigma_{ac} = \sigma_t - \sigma_{dc} = A\omega^S$$

The equation is referred to as universal Jonscher's power law, where A is the temperature-dependent constant determining the magnitude of dispersion at high temperature, and S is the power law exponential term, which varies between 0 and 1. It is essential in determining the possible conduction mechanism in the material and is obtained from the slope of $\ln\sigma_{ac}$ against $\ln\omega$ at high frequencies. If the value of S comes out to be lower than unity and it decreases with temperature, then the mechanism possible is the correlated barrier hopping (CBH) conduction. In this mechanism, ac-conductivity shows exponential variation with temperature, and charge carriers hop between sites over a potential barrier separating them. The maximum barrier height is related to S according to the following relation[41,42]

$$S = 1 - \frac{6k_BT}{W_{max}}$$

In the present PPy/$(PhSe)_2$ nanocomposite material, ac-conductivity varies with temperature exponentially being lower at low temperatures and then rises exponentially with an increase in temperature [Figure 6e,f]. From the plot of $\ln\sigma_{ac}$ against $\ln\omega$ at high frequencies as shown in Figure 7b, the exponent S for the nanocomposite has been found to be 0.31 at room temperature, which is very lower than unity, and is hence indicative of the correlated barrier hopping (CBH) mechanism and involves multiple hopping of charge carriers.[39] This can be envisioned by the fact that conducting PPy represents a potential well from where the charge carriers (electrons) hop to cross the insulating $(PhSe)_2$ energy barrier. The value of maximum barrier height (W_{max}) from the above equation has been found to be 0.224 eV.

The plot of $\ln\sigma_{ac}$ against the inverse of temperature, i.e., $1000/T$ (Figure 7c) clearly revealed almost a linear variation, suggesting that the charge carriers in the nanocomposite material are thermally activated. Moreover, as the variation is linear, the nanocomposite material follows the Arrhenius law, i.e.,

$$\sigma_{ac} = \sigma_o \exp\left(-\frac{E_{ac}}{k_BT}\right)$$

The ac-activation barrier (E_{ac}) is obtained from the slope of the linear plot at various frequencies (0.2, 0.4, 0.6, and 0.8 MHz). The values of E_{ac} obtained are plotted against frequency, as shown in Figure 7d, which exhibited a decreasing trend, thereby reflecting the contribution of frequency to conduction and further confirming the dominance of the hopping mechanism. The decrease in E_{ac} with frequency also justifies the increased ac-conductivity owing to facile hopping of charge carriers.[39]

2.7. Resistance-Temperature Behavior. The resistance-temperature behavior of the PPy/$(PhSe)_2$ nanocomposite, as shown in Figure 8a, exhibits an exponential decrease in resistance with an increase in temperature up to a certain

https://dx.doi.org/10.1021/acsomega.0c05799
ACS Omega 2021, 6, 7413−7421

Scheme 2. Schematic Representation of the PPy/$(PhSe)_2$ Nanocomposite

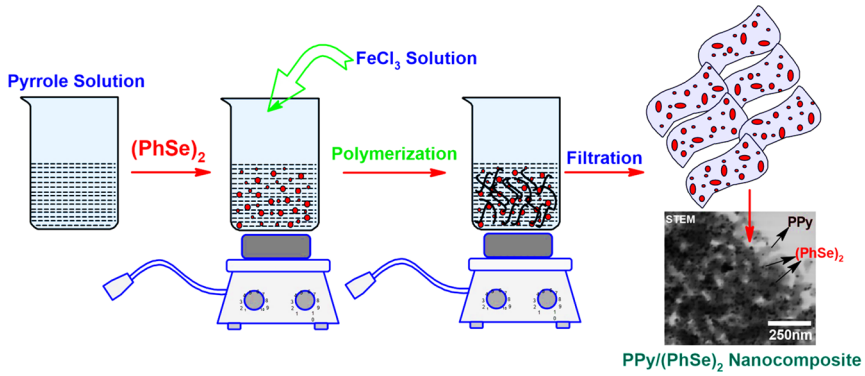

critical temperature (T_c), which is then followed by an abrupt increase. This is a clear indication that the present nanocomposite material behaves like a switching-type positive temperature coefficient (PTC) thermistor. The critical temperature (T_c) has been found to be 401 K, before which the nanocomposite material behaves like an NTC (negative temperature coefficient) system and above which there is a dramatic increase in resistance with increasing temperature, thus reflecting a PTC behavior. The material with such a behavior has been classified into the category of a switching-type PTC material, which finds application mainly in self-regulating heaters.

In the NTC regime, the value of B (a material constant expressing the degree of thermistor sensitivity having temperature units) is obtained from the plot of ln$R$ against the inverse of temperature ($1/T$), in the temperature range of ambient to 400 K, as per the following equation

$$R = Ae^{B/T}$$

where A is another constant. The value of B has been found to be 820.85 K (0.07 eV) at low resistances, which is lower than those of typical NTC materials (around 2600 K at low resistances and 5000 K at high resistances) indicating lower sensitivity. This is obvious since the nanocomposite does not form a typical NTC material but rather a switching-type PTC system wherein a smaller NTC effect is usually observed up to a critical temperature (Curie temperature). Moreover, the value of B in eV measures activation energy that was found to be 0.07 eV. This activation energy is almost similar to that obtained from ac-conductivity data though a bit lower at lower frequencies. Clearly, the charge transport via hopping is thermally activated so as to cross the maximum barrier height of 0.224 eV. Other parameters obtained such as the NTC intensity (I_{NTC}), the temperature coefficient of resistance (α_T), and the sensitivity coefficient (SC), in the temperature range of ambient to 400 K, corresponding to the NTC regime are shown in Table 1.[19,20]

The resistance-temperature behavior of the PPy/$(PhSe)_2$ nanocomposite material can be explained by the hopping mechanism as has already been proven in the dielectric section. Higher resistances at ambient temperatures can be attributed to the presence of a dielectric filler as an insulating barrier in between the conducting PPy chains. As heating occurs, resistance decreases, which might be due to the reordering and expansion of the PPy matrix such that the interaction between $(PhSe)_2$ nanoparticles with PPy chains is facilitated. This reordering and the interaction that hold the PPy chains close together allow for the facile flow of current via hopping of charge carriers. However, above 400 K, the abrupt increase in resistance with rise of temperature may be due to the disruption of PPy chains that inhibits the conduction. This disruption of PPy chains above 400 K is in accordance with TG data. This is schematically shown in Scheme 1a,b.

3. CONCLUSION

The synthesized PPy/$(PhSe)_2$ nanocomposite has been found to show a colossal value of the dielectric constant and exhibit a normal dispersion behavior with changing frequency. With respect to temperature variation, the dielectric data exhibit an increasing trend. This is due to the increase in material movement as temperature rises. Impedance and modulus formalism show one semicircular arc in Cole−Cole plots, which is indicative of single relaxation. A smaller arc in the case of the nanocomposite as compared to PPy suggests higher conductivity of the nanocomposite. Conduction in the nanocomposite has been found to follow the correlated barrier hopping (CBH) model wherein charge carriers hop over an insulating $(PhSe)_2$ barrier. Reduction in the activation energy for hopping has been observed with rise of frequency from 0.2 to 0.8 MHz. From the resistance-temperature behavior, a switching-type PTC behavior has been observed with a Curie temperature of 400 K. Below 400 K, there is a smaller NTC effect (lower B value), while above this temperature, a strong PTC effect is reflected. This might be due to the expansion of PPy chains upon heating, thereby reducing the barrier height to facilitate current flow. However, above 400 K, disruption of PPy chains allows to reflect a PTC behavior.

4. EXPERIMENTAL SECTION

4.1. Materials and Physical Measurements. Pyrrole (Himedia, India) was distilled and stored at −5 °C prior to use. Diphenyl diselenide [$(PhSe)_2$, Sigma Aldrich, India], anhydrous ferric chloride ($FeCl_3$, Fisher Scientific, India), and chloroform ($CHCl_3$, Fisher Scientific, India) used were of analytical reagent grade. The structural characterization of samples was performed by X-ray diffraction (XRD) using a PW 3050 diffractometer (Cu Kα radiation, λ = 1.5418 Å). Fourier transform infrared spectroscopy (FTIR) was performed on a PerkinElmer RX-1 FTIR spectrophotometer in the range of 4000−500 cm^{-1}. The thermal properties were measured by thermogravimetric analysis (TGA) performed on a SEIKO TG/DTA 6200 machine at a heating rate of 10 °C/min under N_2. Dielectric studies of synthesized samples were performed using a computer-controlled LCR meter analyzer (Model

https://dx.doi.org/10.1021/acsomega.0c05799
ACS Omega 2021, 6, 7413−7421

Agilent 4285). Particle size and morphology of synthesized nanocomposites have been characterized by scanning transmission electron microscopy (STEM, Hitachi H-9500).

4.2. Synthesis of the PPy/$(PhSe)_2$ Nanocomposite. Pristine PPy has been synthesized as per the standard procedure.[43] The PPy/$(PhSe)_2$ nanocomposite has been prepared by in situ chemical oxidative polymerization. $(PhSe)_2$ (1 g) has been dispersed uniformly in 0.3 M nonaqueous solution ($CHCl_3$) of a pyrrole monomer. While stirring, 0.6 M solution of $FeCl_3$ in $CHCl_3$ has been added dropwise into the above dispersed mixture at room temperature. As soon as $FeCl_3$ solution is added, the reaction mixture turned black, which indicated the immediate polymerization of the pyrrole monomer. The reaction mixture was stirred for about 5 h for effective polymerization. During polymerization, the PPy chains engulf $(PhSe)_2$ particles to form the nanocomposite. The black colored precipitate of the PPy/$(PhSe)_2$ nanocomposite has been collected by filtration. The material was thoroughly washed with $CHCl_3$ and then dried in an oven at around 40−50 °C to a constant yield. This is schematically shown in Scheme 2.

AUTHOR INFORMATION

Corresponding Authors

Masood Ahmad Rizvi − *Department of Chemistry, University of Kashmir, Srinagar 190006, J&K, India*; Email: masoodku2@gmail.com

Mohd Hanief Najar − *Department of Chemistry, Government College of Engineering & Technology, Safapora 193504, J&K, India*; orcid.org/0000-0002-4107-8483; Phone: 7006870228; Email: haniefarf@gmail.com

Authors

Tabee Jan − *Department of Chemistry, University of Kashmir, Srinagar 190006, J&K, India*

Syed Kazim Moosvi − *School Education Department, Srinagar 190001, J&K, India*

Sajjad Husain Mir − *School of Chemistry, Trinity College Dublin, The University of Dublin, Dublin 2, Ireland*

Ghulam Mustafa Peerzada − *Department of Chemistry, University of Kashmir, Srinagar 190006, J&K, India*

Complete contact information is available at: https://pubs.acs.org/10.1021/acsomega.0c05799

Notes

The authors declare no competing financial interest.

ACKNOWLEDGMENTS

The authors are grateful to the Head, Prof. Syed Wajaht Amin Shah, Department of Chemistry, University of Kashmir for providing constant encouragement and motivation to carry out this research work.

REFERENCES

(1) Zhang, X.; Zhang, J.; Xia, L.; Wang, J.; Li, C.; Xu, F.; Zhang, X.; Wu, H.; Guo, S. Achieving high-efficiency and robust 3D thermally conductive while electrically insulating hybrid filler network with high orientation and ordered distribution. *Chem. Eng. J.* **2018**, *334*, 247−256.

(2) Dar, M. A.; Kotnala, R. K.; Verma, V.; Shah, J.; Siddiqui, W. A.; Alam, M. High Magneto-Crystalline Anisotropic Core−Shell Structured $Mn_{0.5}Zn_{0.5}Fe_2O_4$/Polyaniline Nanocomposites Prepared by in Situ Emulsion Polymerization. *J. Phys. Chem. C* **2012**, *116*, 5277−5287.

(3) Zhao, B.; Zhao, C.; Li, R.; Hamidinejad, S. M.; Park, C. B. Flexible, Ultrathin, and High-Efficiency Electromagnetic Shielding Properties of Poly(Vinylidene Fluoride)/Carbon Composite Films. *ACS Appl. Mater. Interfaces* **2017**, *9*, 20873−20884.

(4) Arjmand, M.; Mahmoodi, M.; Gelves, G. A.; Park, S.; Sundararaj, U. Electrical and electromagnetic interference shielding properties of flow-induced oriented carbon nanotubes in polycarbonate. *Carbon* **2011**, *49*, 3430−3440.

(5) Wang, Y.; Hao, J.; Huang, Z.; Zheng, G.; Dai, K.; Liu, C.; Shen, C. Flexible electrically resistive-type strain sensors based on reduced graphene oxide-decorated electrospun polymer fibrous mats for human motion monitoring. *Carbon* **2018**, *126*, 360−371.

(6) Liu, H.; Gao, J.; Huang, W.; Dai, K.; Zheng, G.; Liu, C.; Shen, C.; Yan, X.; Guo, J.; Guo, Z. Electrically conductive strain sensing polyurethane nanocomposites with synergistic carbon nanotubes and graphene bifillers. *Nanoscale* **2016**, *8*, 12977−12989.

(7) Liu, H.; Huang, W.; Yang, X.; Dai, K.; Zheng, G.; Liu, C.; Shen, C.; Yan, X.; Guo, J.; Guo, Z. Organic vapor sensing behaviors of conductive thermoplastic polyurethane−graphene nanocomposites. *J. Mater. Chem. C* **2016**, *4*, 4459−4469.

(8) Pang, H.; Xu, L.; Yan, D. X.; Li, Z.-M. Conductive polymer composites with segregated structures. *Prog. Polym. Sci.* **2014**, *39*, 1908−1933.

(9) Goda, E. S.; Gab-Allah, M. A.; Singu, B. S.; Yoon, K. R. Halloysite nanotubes based electrochemical sensors: A review. *Microchem. J.* **2019**, *147*, 1083−1096.

(10) Goda, E. S.; Lee, S.; Sohail, M.; Yoon, K. R. Prussian blue and their analogues as advanced supercapacitor electrodes. *J. Energy Chem.* **2020**, *50*, 206−229.

(11) Goda, E. S.; Yoon, K. R.; El-sayed, S. H.; Hong, S. E. Halloysite Nanotubes as Smart Flame retardant and economic reinforcing materials : A review. *Thermochim. Acta* **2018**, *669*, 173−184.

(12) Goda, E. S.; Hong, S. E.; Yoon, K. R. Facile Synthesis of Cu-PBA nanocubes/Graphene oxide Nanocomposite as Binder-free Electrodes for Supercapacitor. *J. Alloys Compd.* **2021**, 157868.

(13) Deng, H.; Skipa, T.; Bilotti, E.; Zhang, R.; Lellinger, D.; Mezzo, L.; Fu, Q.; Alig, I.; Peijs, T. Preparation of High-Performance Conductive Polymer Fibers through Morphological Control of Networks Formed by Nanofillers. *Adv. Funct. Mater.* **2010**, *20*, 1424−1432.

(14) Bao, S. P.; Liang, G. D.; Tjong, S. C. Effect of mechanical stretching on electrical conductivity and positive temperature coefficient characteristics of poly(vinylidene fluoride)/carbon nanofiber composites prepared by non-solvent precipitation. *Carbon* **2011**, *49*, 1758−1768.

(15) Chu, K.; Lee, S. C.; Lee, S.; Kim, D.; Moon, C.; Park, S. H. Smart conducting polymer composites having zero temperature coefficient of resistance. *Nanoscale* **2015**, *7*, 471−478.

(16) Jeon, J.; Lee, H. B. R.; Bao, Z. Flexible wireless temperature sensors based on Ni microparticle-filled binary polymer composites. *Adv. Mater.* **2013**, *25*, 850−855.

(17) Kono, A.; Shimizu, K.; Nakano, H.; Goto, Y.; Kobayashi, Y.; Ougizawa, T.; Horibe, H. Positive-temperature-coefficient effect of electrical resistivity below melting point of poly(vinylidene fluoride) (PVDF) in Ni particle-dispersed PVDF composites. *Polymer* **2012**, *53*, 1760−1764.

(18) Chu, K.; Park, S. H. Electrical heating behavior of flexible carbon nanotube composites with different aspect ratios. *J. Ind. Eng. Chem.* **2016**, *35*, 195−198.

(19) Cui, X.; Chen, J.; Zhu, Y.; Jiang, W. Lightweight and conductive carbon black/chlorinated poly(propylene carbonate) foams with a remarkable negative temperature coefficient effect of resistance for temperature sensor applications. *J. Mater. Chem. C* **2018**, *6*, 9354−9362.

(20) Zhao, S.; Lou, D.; Zhan, P.; Li, G.; Dai, K.; Guo, J.; Zheng, G.; Liu, C.; Shen, C.; Guo, Z. Heating-induced negative temperature coefficient effect in conductive graphene/polymer ternary nano-

composites with a segregated and double-percolated structure. *J. Mater. Chem. C* **2017**, *5*, 8233−8242.
(21) Xiang, Z.-D.; Chen, T.; Li, Z.-M.; Bian, X.-C. Negative Temperature Coefficient of Resistivity in Lightweight Conductive Carbon Nanotube/Polymer Composites. *Macromol. Mater. Eng.* **2009**, *294*, 91−95.
(22) He, X. J.; Du, J. H.; Ying, Z.; Cheng, H. M.; He, X. J. Positive temperature coefficient effect in multiwalled carbon nanotube/high-density polyethylene composites. *Appl. Phys. Lett.* **2005**, *86*, 62112−62114.
(23) Majid, K.; Awasthi, S.; Singla, M. L. Low temperature sensing capability of polyaniline and Mn_3O_4 composite as NTC material. *Sens. Actuators, A* **2007**, *135*, 113−118.
(24) da Silva, G. T. S. T.; Michels, F. S.; Silveira, R. G.; Caires, A. R. L.; Casagrande, G. A. Insights into the electronic properties of diphenyl chalcogenides compounds: A combined experimental and theoretical study. *J. Mol. Struct.* **2019**, *1185*, 21−26.
(25) Khan, A. A.; Hussain, R.; Baig, U. DC electrical conductivity and rate of ammonia vapour-sensing performance of synthetic polypyrrole−zirconium(IV) phosphate cation exchange nanocomposite. *Int. J. Ind. Chem.* **2017**, *8*, 157−173.
(26) Junior, O. D. R. A.; Antônio, E.; Mainardes, R. M.; Khalil, N. M. Preparation, physicochemical characterization and antioxidant activity of diphenyl diselenide-loaded poly(lactic acid) nanoparticles. *J. Trace Elem. Med. Biol.* **2017**, *39*, 176−185.
(27) Marsh, R. E. The crystal structure of diphenyl diselenide. *Acta Cryst.* **1952**, *5*, 458−462.
(28) Moosvi, S. K.; Naqash, W.; Najar, M. H.; et al. Current−voltage characteristics and thermal studies of polypyrrole-octacyanotungstate composite. *Mater. Res. Innovations* **2020**, 1.
(29) Najar, M. H.; Majid, K. Enhanced photo-catalytic activity exhibited by PTh/$[Fe(CN)_3$ $(NO)(bpy)]\cdot 4H_2O$ nanocomposite fibers via a synergistic approach. *RSC Adv.* **2015**, *5*, 107209−107221.
(30) Adnan, S. B. R. S.; Mohamed, N. S. AC conductivity and dielectric studies of modified Li_4SiO_4 ceramic electrolytes. *Ceram. Int.* **2014**, *40*, 11441−11446.
(31) Prabakar, K.; Narayandass, S. K.; Mangalaraj, D. Dielectric and electric modulus properties of vacuum evaporated $Cd_{0.8}Zn_{0.2}Te$ thin films. *Mat. Sci. Eng. B* **2003**, *98*, 225−231.
(32) Lakhdar, M. H.; Ouni, B.; Amlouk, M. Dielectric relaxation, modulus behavior and conduction mechanism in Sb_2S_3 thin films. *Mater. Sci. Semicond. Process.* **2014**, *19*, 32−39.
(33) Najar, M. H.; Majid, K. Investigation of the transport properties of PPy/[Co(EDTA) (NH_3) Cl] H_2O nanocomposite prepared by chemical oxidation method. *RSC Adv.* **2016**, *6*, 25449−25459.
(34) Najar, M. H.; Majid, K.; Dar, M. A. Electric modulus based relaxation dynamics, ac-conductivity and I−V characteristics in PTh/[Co(EDTA)NH_3Cl] H_2O nanocomposite prepared by chemical oxidation method. *J. Mater. Sci.: Mater. Electron.* **2017**, *28*, 11243−11252.
(35) Singh, L.; Kim, I. W.; Sin, B. C.; Ullah, A.; Woo, S. K.; Lee, Y. Study of dielectric, AC-impedance, modulus properties of $0.5Bi_{0.5}Na_{0.5}TiO_3$. $0.5CaCu_3Ti_4O_{12}$ nano-composite synthesized by a modified solid state method. *Mater. Sci. Semicond. Process.* **2015**, *31*, 386−396.
(36) Shekharam, T.; Rao, V. L.; Yellaiah, G.; Kumar, T. M.; Nagabhushanam, M. AC conductivity, dielectric and impedance studies of $Cd_{0.8-x}Pb_xZn_{0.2}S$ mixed semiconductor compounds. *J. Alloy Compd.* **2014**, *617*, 952−960.
(37) Najar, M. H.; Majid, K.; Dar, M. A. Dielectric and impedance spectroscopic analysis in SNP-d embedded PTh nano rods for energy storage applications. *Synth. Met.* **2020**, *268*, 116485.
(38) Dar, M. A.; Majid, K.; Batoo, K. M.; Kotnala, R. K. Dielectric and impedance study of polycrystalline $Li_{0.35\_0.5X}Cd_{0.3}Ni_XFe_{2.35\_0.5X}O_4$ ferrites synthesized via a citrate-gel auto combustion method. *J. Alloy Compd.* **2015**, *632*, 307−320.
(39) Hazarika, J.; Kumar, A. Electric modulus based relaxation dynamics and ac conductivity scaling of polypyrrole nanotubes. *Synth. Met.* **2014**, *198*, 239−247.
(40) Najar, M. H.; Majid, K. Synthesis and characterization of nanocomposite of polythiophene with $Na_2[Fe(CN)_3(OH)(NO)$-$C_6H_{12}N_4]$ H_2O: a potent material for EMI shielding applications. *J. Mater. Sci.: Mater. Electron.* **2015**, *26*, 6458.
(41) Tabib, A.; Sdiri, N.; Elhouichet, H.; Férid, M. Investigations on electrical conductivity and dielectric properties of Na doped ZnO synthesized from sol gel method. *J. Alloy Compd.* **2015**, *622*, 687−694.
(42) Najar, M. H.; Majid, K. Nanocomposite of polypyrrole with the nano-photoadduct of sodium pentacyanonitrosylferrate(II) dihydrate and EDTA: A potential candidate for capacitor and a sensor for HF radio wave detection. *Synth. Met.* **2014**, *198*, 76−83.
(43) Rizvi, M. A.; Moosvi, S. K.; Jan, T.; Bashir, S.; Kumar, P.; Roos, W. D.; Swart, H. C. Dielectric, magnetic and photocatalytic activity of PolyPyrrole/Prussian red nanocomposite for waste water treatment applications. *Polymer* **2019**, *163*, 1−12.

https://dx.doi.org/10.1021/acsomega.0c05799
ACS Omega 2021, 6, 7413−7421